Magnetic Resonance Imaging, Vol. 16, Nos. 5/6, pp. 455–461, 1998

Printed in the USA.
0730-725X/98 $19.00 + .00

PII S0730-725X(98)00072-1

● *Invited Lecture*

A BROAD LINE NMR AND MRI STUDY OF WATER AND WATER TRANSPORT IN PORTLAND CEMENT PASTES

A.J. BOHRIS,* U. GOERKE,* P.J. MCDONALD,* M. MULHERON,† B. NEWLING,* AND B. LE PAGE†

Schools of *Physical Sciences and †Chemical, Civil and Environmental Engineering, University of Surrey, Guildford, Surrey, UK

The results of a magnetic resonance spin-spin relaxation analysis and broad-line magnetic resonance imaging (MRI) (gradient-echo and stray-field imaging) study of water and water transport in Portland cement pastes are presented. The effect of varying the cure conditions and the water to cement (w/c) ratio of the sample mix are discussed. The water sorptivity and the concentration dependence of the hydraulic diffusion coefficient are calculated for samples prepared with a 0.5 w/c ratio and, therefore, an open pore structure. In the case of 0.3 w/c ratio samples, little water transport is observed, and a closed pore structure is inferred. © 1998 Elsevier Science Inc.

Keywords: **Cement; Diffusion; Water; stray field imaging (STRAFI); Magnetic resonance imaging; Relaxation.**

INTRODUCTION

It is well known that the presence of water and water transport play key roles in determining the pore structure and long term durability of cementitious materials. However, despite the undoubted economic importance of cement and the very large volume of previous analysis of the problem, the details of this role remain poorly understood. The traditional techniques available for characterizing water content and transport in cement are largely inadequate, in that they are either destructive or invasive, thus prohibiting time-course studies, or are lacking in spatial resolution. Proton magnetic resonance imaging (MRI), is both nondestructive and noninvasive and is spatially resolved. Moreover, it is particularly sensitive to water dynamics. The earliest report of the use of MRI in this context is by Gummerson et al.[1] Other examples include work by Papavassiliou et al.,[2] Kaufmann and Studer,[3] and Fordham et al.[4] To date, however, a severely limiting factor has been that resonance line widths in cements are very broad. Consequently, only the most mobile water in the largest capillaries, cracks, and voids has been observed. The broad nuclear magnetic resonance (NMR) line widths can be attributed to a number of causes, among which are diffusive broadening due to self-diffusion in the large magnetic-field gradients caused by inhomogeneity of the magnetic susceptibility across pore surfaces and around paramagnetic impurities, and fast exchange with strongly relaxing surface sites. Only more recently have broad line imaging techniques been employed.[5–8]

Surface relaxivity has been exploited by Halperin et al.[9] using the complementary technique of magnetic resonance relaxometry. These authors show that the initial ^{1}H spin-spin relaxation time (T_2) of water in a cured 0.43 water to cement (w/c) ratio cement paste varies according to water content, indicating that the rapid exchange model of relaxation can be applied to determine the pore surface area to volume ratio. Distributed exponential fitting of decay curves yields the pore-size distribution, which is shown to be strongly bimodal. Later cryoporometry experiments by the same group[10] revealed a small additional volume of larger capillary pores. In arriving at these pore sizes no account was taken of the surface roughness, an issue considered at some length by Papavassiliou et al.[11] in the context of spin-lattice (T_1) relaxation.

This paper presents the results of an NMR T_2 relaxation and broad-line MRI study of the hydration and curing of cement pastes and of subsequent water transport in cured material. Water to cement ratios in the

Address correspondence to Dr. P.J. McDonald, School of Physical Sciences, University of Surrey, Guildford, Surrey, GU2 5XH, UK

range 0.26–0.60 have been studied, although only results for w/c ratios of 0.3 and 0.5 are presented here. Samples have been cured in open, sealed, or underwater environments. The objective is to correlate the bulk relaxation analysis of samples sealed during cure, which are assumed to be spatially uniform, with the structure of the paste based on traditional understanding.[12,12a] Quantitative broad-line imaging is then used to observe deviations from this model in the case of samples cured open or underwater where spatial heterogeneity is expected. After cure, samples have been dried and/or exposed to further water to investigate the water uptake properties of the cured material. Where appropriate, hydraulic diffusivities have been determined.

Cement Chemistry

Dry Portland cement powder[12,12a] is composed of various calcium silicates and aluminates with small additional fractions of gypsum, (calcium sulphate), and has a relative density of 3.1. When it is mixed with water, it immediately starts to hydrate. Calcium silicate hydrate (CSH) and calcium alumino sulphate hydrate form on the surfaces of the particles, and crystals of calcium hydroxide precipitate out from the saturated solution. With time, a layered network of CSH, known as the gel, is formed. Cements differ, but as a rule of thumb, Portland cement requires 40% its own weight of water to fully hydrate. Of this, 25% is required for chemical reactions, is nonevaporable, and undergoes shrinkage equivalent to 25% its volume. The other 15%, known as gel water, is adsorbed onto the internal surfaces of the gel and is evaporable under extreme conditions. The shrinkage of the gel creates voids, known as capillaries, which, dependent on conditions, may or may not form a connected network. Excess water not required for hydration occupies further capillaries, while, if there is insufficient water, unreacted cement remains. Capillary water is readily evaporable from a connected pore network. Figure 1 illustrates these general considerations for the w/c ratios 0.3 and 0.5, which straddle the critical 40%. The above arguments assume that the sample is sealed; if it is left open during the cure, then some drying will occur. Alternatively, if the cement is cured underwater, then capillary voids may fill with water.

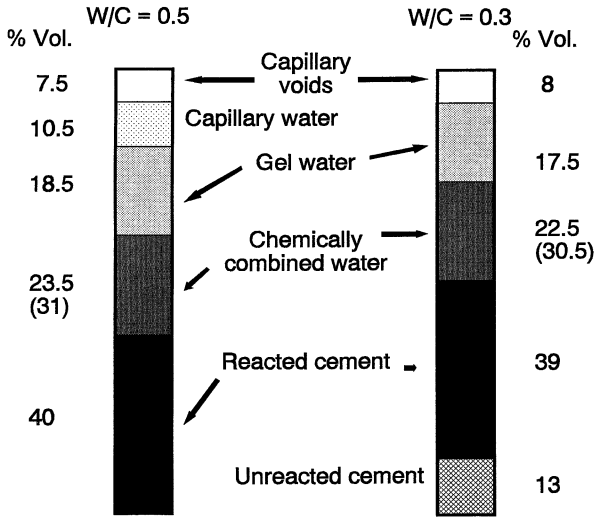

Fig. 1. The calculated percentile volumes of different components in fully hydrated Portland cement pastes prepared with w/c ratios of 0.5 (left) and 0.3 (right). The combined water has undergone 25% shrinkage; its original percentile volume is shown in brackets (after Ref. 12 and 12a).

EXPERIMENTAL

Cement paste samples were studied using bulk relaxometry, including free induction decay and Carr–Purcell–Meiboom–Gill (CPMG) analysis, gradient-echo imaging,[13] and stray-field imaging.[14] The bulk relaxation analysis was carried out at 20 MHz. A short pulse gap of 100 μs was used for the CPMG experiments to minimize the effects of water diffusion in the susceptibility gradients. The gradient-echo imaging was conducted at 30 MHz, using both the standard method and a steady state variant[15] with an echo time (gradient period) of 216 μs and a gradient strength of 30 G/cm. The NMR frequency, echo time (2τ), and gradient strength for the stray-field imaging were 235 MHz, 50 μs, and 5800 G/cm, respectively. A multiple quadrature echo train was recorded.

For most of the studies, cement paste samples were cast in glass pots and NMR tubes from Portland cement (Cement Manufacturers Federation standard grade) using a food processor to mix the water and cement powder and a vibration table to remove incorporated air. The tubes and pots were sealed. In the case of samples cured underwater, additional water was carefully added to the pots after vibration and before closure. For the measurements made during cure, the samples were examined *in situ*. For the subsequent imaging of water uptake by gradient-echo imaging, the samples were removed from the glass using a diamond saw, and the sides were sealed with waxed film. The samples were then placed on a water-saturated sponge with the original upper surface remaining at the top, away from the sponge. The samples were temporarily removed from the sponge for imaging. In the case of stray-field imaging, poly(methyl methaorylate) (PMMA) moulds were used for curing, and the cured samples were subsequently glued into glass tubes using epoxy. Water was added at the top. Where necessary, samples were dried using repeated cycles of methanol exchange and moderate oven drying at temperatures up to 50°C. This procedure was adopted to minimize

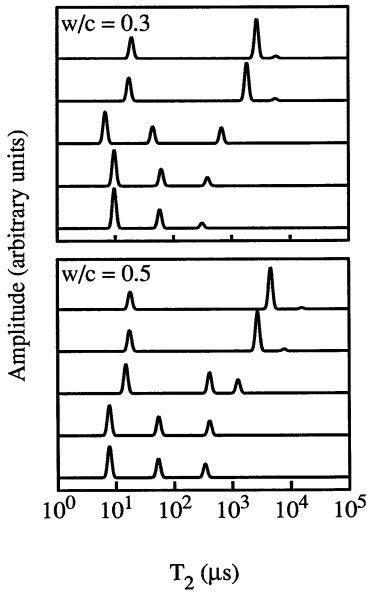

Fig. 2. The three-component T_2 analyses of sealed cement pastes prepared with 0.5 and 0.3 w/c ratios. The traces, from the top, are for 1 and 4 h and 1, 8, and 28 days. The amplitudes of the peaks represent the amplitudes of the different T_2 components. The widths, fixed at ±7.5% of T_2, are typical of distributions found over three repeat samples.

damage to the pore structure. The sample weights were monitored at all stages of the experiment.

RESULTS AND DISCUSSION

Relaxation Analysis of Curing

Figure 2, a and b, shows the development over 28 days of the multicomponent T_2-relaxation profile of cement paste samples prepared with w/c ratios of 0.5 and 0.3, respectively. The results shown for each w/c ratio are the average of three samples. In every case an attempt was made to fit both two- and three-component exponentials to the data. While distributed exponentials more accurately reflect distributed pores sizes, previous experience[9,11] has generally led to strongly bi- and trimodal T_2 distributions depending on whether chemically combined water is included. These can be reasonably approximated by simple two- or three-component fits so as to fulfill the primary objective of identifying the chemically combined gel and capillary water. In support of this, we noted a high degree of reproducibility between samples and between different fitting algorithms.

For samples with both 0.3 and 0.5 w/c ratios, the presence of about one-third of the proton signal in a short T_2 component of 20 μs after just 1 h is evidence that a substantial degree of hydration takes place during the early stages of cure. At this time, the remaining water is predominantly in a single, longer component characteristic of mobile water. In the case of the 0.5 w/c ratio samples, there is a clear evolution over the subsequent time course toward three components with T_2 values of approximately 9, 80, and 350 μs in the amplitude ratios 0.5:0.3:0.2, respectively. Based on the forgoing discussion, the short component is associated with chemically combined water, the middle component with gel water, and the long component with capillary water. These components are expected to be in the amplitude ratio 31:18.5:10.5 (Fig. 1) or equivalently 0.52:0.31:0.17, in excellent agreement with experiment. In the case of the 0.3 w/c ratio samples, the importance of the capillary water is somewhat different. After about 1 day of curing, separate chemically combined, gel and capillary water signals can be discerned with intensity ratios of 0.5:0.25:0.25, respectively. However, as curing proceeds beyond this, the fraction of capillary water is much reduced, and the combined to gel water ratio tends to about 2:1, in broad agreement with theory. The capillary water signal is not, however, zero after 28 days as might be expected, suggesting that cure of this sample remains incomplete.

The gel pores are formed between layers of CSH. Therefore, according to the fast-exchange model of relaxation[16] the observed relaxation time of gel water, T_2^{obs}, is expected to be given by:

$$\frac{1}{T_2^{obs}} \approx \frac{\lambda}{d T_2^s} \tag{1}$$

where T_2^s is the relaxation time of surface adsorbed water, λ is the thickness of a water layer (3 Å), and d is the thickness of the gel water layer between the CSH sheets. If T_2^s is equated with the relaxation time of the chemically combined water, taken as 10 μs, and T_2^{obs} is taken as 80 μs, then d is 24 Å, in good agreement with earlier NMR relaxometry work[9,10] and accepted values.[12,12a] It is more difficult to evaluate the capillary pore size, since there is less certainty that the capillary pores are completely filled. On the assumption that they are approximately two-thirds full (Fig. 1) and spherical, then the radius evaluates to approximately 150 Å, in agreement with earlier NMR results but smaller than accepted values. The discrepancy may be caused by the water aggregating in the void interstices or by self-diffusion in susceptibility gradients, which even at τ = 100 μs in the CPMG experiment may cause significant signal attenuation. Alternatively, the discrepancy may be due to a failure to account for the pore-surface roughness.

Gradient-Echo Imaging of Curing

The profiles in Fig. 3 are of a 0.5 w/c ratio sample

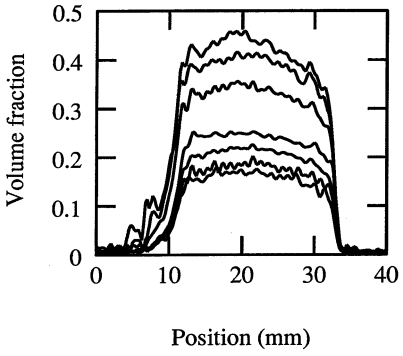

Fig. 3. The time evolution of the capillary water profile in a 0.5 w/c ratio cement paste during sealed curing. The profiles, from the top, are recorded after 6 and 12 h and 1, 3, 7, 14, and 28 days.

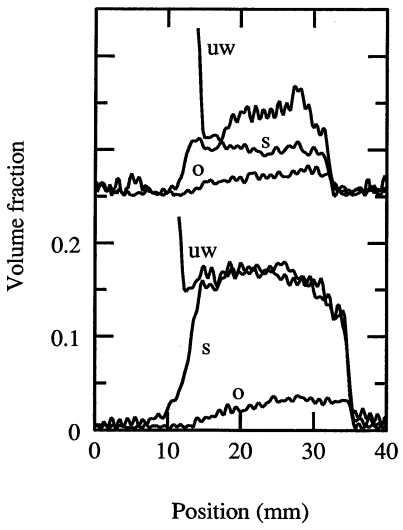

Fig. 4. The 28-day capillary water profiles of the 0.5, lower traces, and 0.3, upper traces (×3), w/c ratio cement pastes cured under sealed conditions (s) compared to those cured open (o) and underwater (uw). The open/water saturated tops of the samples are to the left.

cured under sealed conditions in which the curing is expected to be spatially uniform. The echo time of 216 μs used to record the profiles is more than twice the T_2 of the gel water and about half that of the capillary water. Consequently, the profile intensities, which have been normalised to a standard sample so as to reflect volume fraction of water, primarily reflect the capillary water in the samples. A gradual and approximately spatially uniform decrease in the volume of mobile water is observed throughout the time course of the experiment, broadly consistent with expectations. There is a reduction in signal intensity at the base of the sample (right side), particularly in the early stages, which is attributed to sedimentation. A complementary volume of bleed water is seen at the top, caught in the neck of the sample pot, which is horizontal for the duration of the imaging experiment. The final volume of capillary water is somewhat greater than that predicted by the foregoing discussion and at between 15–20% is suggestive of the capillary voids also being saturated. This observation is further discussed below.

The lower set of traces in Fig. 4 compares the profile recorded after 28 days from the sealed sample with those recorded from similar 0.5 w/c ratio samples cured open and underwater. The open cured sample shows much less water overall and generally decreases toward the exposed surface (left side), consistent with drying of the sample throughout the cure period. It is reasonable to expect that a 0.5 w/c ratio mix results in a cement paste with an open pore structure[12,12a] and, in the underwater cured sample, that the void volume should therefore be filled. Consequently, the substantial similarity in measured water content between the samples cured sealed and underwater is at first surprising. While it is conceivable that negative pore pressures or a closed pore structure have resulted in this similarity, we suggest that it is more likely that the bleed water in the sealed sample has acted as a reservoir of additional water and filled the pores in the later stages of cure. The profile intensities of about 17% water volume are consistent with this hypothesis, corresponding well to the calculated total capillary volume (Fig. 1). This argument implies that there is a small w/c ratio gradient across the sealed sample, caused by sedimentation (see above).

The upper set of traces in Fig. 4 show similar 28-day profiles (multiplied by 3) recorded from samples made with a 0.3 w/c ratio mix. The overall level of capillary water is very much reduced, again consistent with the relaxation analysis. As with the 0.5 w/c ratio sample, a concentration gradient is observed in the open cured sample. Unlike the 0.5 w/c ratio samples, however, more water is now observed with underwater curing than with sealed curing, although the difference is considerably less than that required to fill the total void volume. Therefore, we infer a closed pore structure, a result confirmed by the uptake experiments reported below. The reason for the relative lack of water just below the underwater cured sample surface is unclear.

Gradient-Echo Imaging of Water Uptake into Cured Cement

The results of water uptake experiments into 96-day-old sealed, underwater and open cured 0.5 w/c ratio samples are shown in Fig. 5. In every case, the original

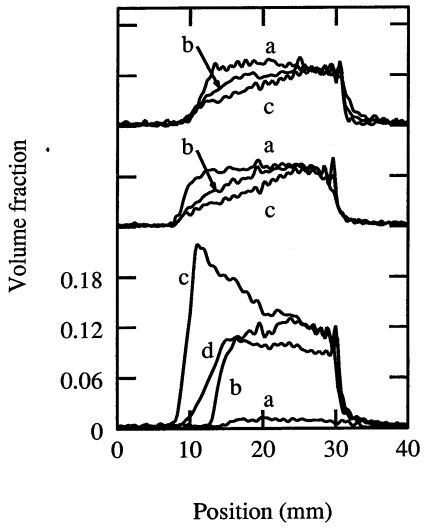

Fig. 5. Capillary water uptake profiles into 96-day-old 0.5 w/c ratio samples. The basal source of water (wet sponge, removed for imaging) is to the right, and the top of each sample is left open. Upper traces show sealed cure after 0 (a), 1 (b), and 7 (c) days of exposure to water. Middle traces show underwater cure after 0 (a), 1 (b), and 7 (c) days of exposure to water. Bottom traces show open cure after 0 (a), 1 (b), and 6 (c) h and 7 days (d) of exposure to water. In each case, the last trace represents a dynamic equilibrium.

base of the sample (right side) was in contact with the wet sponge. The samples cured under sealed and underwater conditions are once again remarkably similar. There is, however, a decrease in the initial level compared to the 28-day profiles. This is mainly attributed to a partial drying of the cement, aggravated by diamond saw cutting of the glass, on removal from the casting pots. Similar decreases were noted in other 28 day samples similarly removed from their pots. More interesting is the fact that, rather than the total water increasing when the cement is placed in contact with the saturated sponge, an overall drying of the sample is observed, with the upper surface showing less water after 24 h than at the start of the experiment. A dynamic equilibrium is reached in which the water profile reflects the balance between evaporation at the top and uptake from the sponge at the base. The fact that this balance is achieved so readily suggests that the pore structure is both open and well connected. Gravitational effects are believed to be negligible in these samples. In the case of the open cured sample, a more surprising result is seen. The water first diffuses into the dry sample with a sharp front. A concentration gradient inverse to that which might be expected rapidly develops, so that the top shows a greater mobile water content. This inverse gradient then recedes over a period of a few days, and a more normal profile is observed. This behaviour is qualitatively explained as follows. During cure, the sample rapidly sets, forming an embryonic pore structure characteristic of a 0.5 w/c ratio paste. However, the sample slowly dries and becomes water deficient, so that cure is substantially incomplete, particularly near the upper surface. This results in a relatively large, unfilled capillary pore volume and explains the low initial water profile. When water is later added, it rapidly fills the voids, giving rise to the inverse concentration gradient. Over the subsequent few days, the additional water hydrates the uncured cement, and the capillary pore volume is reduced. Hence, the water profile diminishes. Unlike the other two samples, the final profile, which reflects a dynamic equilibrium, does not show a constant water-concentration gradient. This implies that there is a pore volume/connectivity gradient across the sample consistent with an inhomogeneous cure.

Almost no water is taken up into 0.3 w/c ratio samples over a period of a few days, and in consequence, the profiles are not included here. This is attributed to the fact that at low w/c ratios the pore structure is largely closed.

Stray-Field Imaging and Diffusion Analysis

Stray-field imaging was used to observe bulk water ingress into sealed cure 0.5 w/c ratio samples that had previously been either air dried, to remove, as far as is possible, all capillary water or dried using methanol exchange to remove capillary and gel water. It is found that the recorded quadrature echoes, which in the case of combined water reflect a degree of line narrowing and in the case of mobile water are strongly diffusion attenuated, can be well represented by two-component exponential decays corresponding in the proportion of their amplitudes to capillary water and to gel and chemically combined water, respectively. Fig. 6 shows a profile of an air-dried sample recorded 1 h after the top was exposed to water. The water reservoir is seen to the left. A sharp water front (solid curve) has ingressed 2.7 mm into the sample. The calculated intensities of the capillary water (lower dashed curve; long T_2 component) and of the gel and combined water (upper dashed curve; short T_2 component) indicate that the advancing water front is capillary water. The details of the front shape are distorted by the finite time required to record the profile. Details of the front shape are better determined in a time of flight experiment (M.R. Halse, private communication) in which the signal intensity is recorded at a fixed location as the front passes. Because data acquisition is considerably more rapid, the distortion is much less. The analysis discussed below uses a combination of time of flight and profile data.

Water transport in cement pastes with a fine pore structure is generally considered to be dominated by

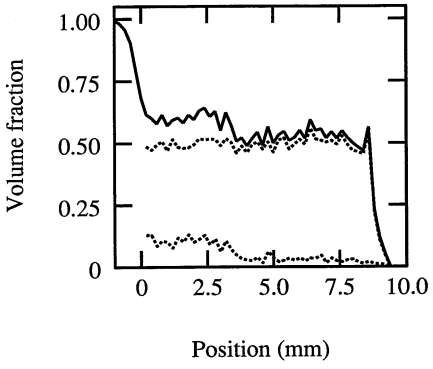

Fig. 6. A stray-field profile (solid line) of a 0.5 w/c ratio cured and air-dried sample exposed to water for 1 h. The dashed traces represent the amplitudes of the long and short T_2 components within the cement. The water reservoir is to the left.

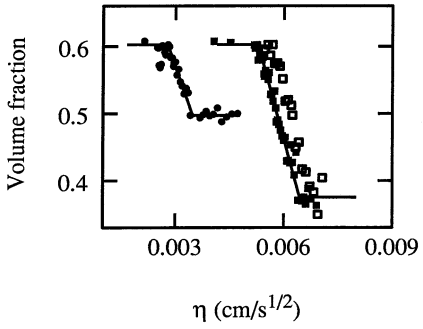

Fig. 7. The master diffusion profiles for water uptake for air-dried (circles) and methanol exchange-dried (squares) samples calculated from profile and time of flight data. The solid lines are fits to the data used to calculate D(c). The open squares are a repeat time-of-flight experiment at a different position.

capillarity. Following earlier work in unsaturated flow theory in soils, Hall[17] has described how water transport in cementitious materials can be modelled as an effective Fickian diffusion process in which the concentration-dependent hydraulic diffusion coefficient is defined as the product of the hydraulic conductivity, κ, and the derivative of the capillary potential, ψ, with respect to water concentration, c. Hence:

$$\frac{\partial c}{\partial t} = \frac{\partial}{\partial x}\left(\mathrm{D}(c)\,\frac{\partial c}{\partial x}\right), \quad \mathrm{D}(c) = \kappa(c)\,\frac{d\psi}{dc} \qquad (2)$$

where x and t are position and time variables, respectively. A feature of generalized Fickian diffusion is that the water front should advance as $t^{1/2}$. We note that this is the case in the experiments reported here. Moreover, for the boundary conditions of these experiments, the hydraulic diffusion coefficient can be calculated from profile and time-of-flight data by applying the Boltzmann transform,[18] $\eta = x/2t^{1/2}$, which results in a single master curve $c(\eta)$. Reworking Eq. (1) yields:

$$\mathrm{D}(c) = \frac{-2\displaystyle\int_{c_0}^{c} \eta(c')\,dc'}{\dfrac{dc}{d\eta}} \qquad (3)$$

where c_0 is the initial, basal level of water in the sample. Figure 7 shows the master diffusion profiles for water ingress into the two differently dried samples collated from the results of multiple profiling and time-of-flight experiments. It is immediately clear that the invading water fractions are in good agreement with expectations (Fig. 1). It is also apparent that water ingresses much more rapidly into the methanol exchange-dried sample than into the air-dried sample. While it is possible that this is due to the additional drying damaging the delicate gel structure of the cement, we believe that the result is significant and reflects the different uptake characteristics of cement to capillary and to combined capillary and gel water. The master curve data have been fitted to three-line trapezoidal functions, which, although physically unrealistic, preserve the essential features of the data. Based on the fits, the diffusion coefficient for capillary water only is calculated to be:

$$\mathrm{D}(c) \approx (10c - 5.1) \times 10^{-5}\ \mathrm{cm^2\,s^{-1}} \qquad 0.6 > \mathrm{c} > 0.5 \qquad (4)$$

and, for combined capillary and gel water:

$$\mathrm{D}(c) \approx (8.7c - 3.4) \times 10^{-5}\ \mathrm{cm^2\,s^{-1}} \qquad 0.6 > \mathrm{c} > 0.4 \qquad (5)$$

where, in both cases, c is expressed in volume fraction of water.

The sorptivity is defined by:

$$\mathrm{S} = 2\int_{c_0}^{c_1} \eta\,dc, \qquad (6)$$

where c_0 and c_1 are the initial and final water concentrations (expressed in mass per unit volume) in the sample. The sorptivity can thus be determined directly from the integral of the $c(\eta)$ master curve. The sorptivity depends on the initial water concentration. From our data, the sorptivity to capillary water of cured 0.5 w/c

ratio cement is 0.66×10^{-3} $cms^{-1/2}$, while for all evaporable water it is 2.7×10^{-3} $cms^{-1/2}$.

In the case of the 0.3 w/c ratio samples, the water uptake into an air-dried sample was minimal, reflecting the closed capillary pore structure. For a methanol exchange-dried sample, extremely rapid uptake was observed. However, in this case, the drying procedure had clearly damaged the pore structure and resulted in microcracking of the sample.

CONCLUSION

It has been shown that the amplitudes of a simple three-component T_2 analysis of cement pastes correlate well with the expected fractional volumes of chemically combined, gel and capillary water. It has further been shown that gradient echo imaging is sufficiently quantitative to provide a reliable, spatially resolved measure of capillary water and that stray-field imaging can quantify all water. The two techniques, used in combination, allow detailed quantitative study of the effects of curing regimens that result in nonuniform curing and the effects of further exposure to water. Differences between the uptake of capillary water and that of combined capillary and gel water have been observed and quantified.

Acknowledgments—The authors thank the UK Science and Engineering Research Council for Research Grant GR/K94881. A.J.B. also thanks the council for a studentship.

REFERENCES

1. Gummerson, R.J.; Hall, C.; Hoff, W.D.; Hawkes, R.; Holland, G.N.; Moore, W.S. Unsaturated water flow within porous materials observed by NMR imaging. Nature 281: 56–57; 1979.
2. Papavassiliou, G.; Milia, F.; Fardis, M.; Rumm, R.; Laganas, E. ^{1}H nuclear magnetic resonance imaging of water diffusion in hardened cement pastes. J. Am. Ceram. Soc. 76:2109–2111; 1993.
3. Kaufmann, J.; Studer, W. One-dimensional water transport in covercrete—application of non-destructive methods. Mat. Struct. 28:115–123; 1995.
4. Fordham, E.J.; Roberts, T.P.L.; Carpenter, T.A.; Hall, L.D.; Maitland, G.C.; Hall, C. Nuclear magnetic resonance imaging of simulated voids in cement slurries. AIChE J. 37:1895–1899; 1991.
5. Nunes, T.; Randall, E.W.; Samoilenko, A.A.; Bodart, P.; Feio, G. The hardening of Portland cement studied by ^{1}H NMR stray field imaging. J. Phys. D Appl. Phys. 29:805–808; 1996.
6. Bogdan, M.; Balcom, B.J.; Bremner, T.W.; Armstrong, R.L. Single-point imaging of partially dried, hydrated white Portland cement. J. Magn. Reson. A116:266–269; 1995.
7. Black, S.; Lane, D.M.; McDonald, P.J.; Mulheron, M.; Hunter, G.; Jones, M.R. The visualisation of the ingress of polymer treatment coatings into porous building materials by stray field magnetic resonance imaging. J. Mat. Sci. Lett. 14:1175–1177; 1995.
8. Bohris, A.J.; Newling, B.; McDonald, P.J. A broad line NMR study of water absorption and transport in fibrous cement roofing tiles. J. Mat. Sci. 33:859–867; 1998.
9. Halperin, W.P.; Jehng, J.-Y.; Song, Y.-Q. Application of spin-spin relaxation to measurement of surface area and pore size distributions in a hydrating cement paste. Magn. Reson. Imaging 12:169–173; 1994.
10. Jehng, J.-Y.; Sprague, D.T.; Halperin, W.P. Pore structure of hydrating cement paste by magnetic resonance relaxation analysis and freezing. Magn. Reson. Imaging 14: 785–791; 1996.
11. Papavassiliou, G.; Fardis, M.; Laganas, E.; Leventis, A.; Hassanien, A.; Milia, F.; Papageorgiou, A.; Chaniotakis, E. Role of surface morphology in cement gel growth dynamics: a combined nuclear magnetic resonance and atomic force microscopy study. J. Appl. Phys. 82:449–452; 1997.
12. Czernan, W. Cement Chemistry and Physics for Civil Engineer, chap. 3. London: Crosby Lockwood and Son Ltd., 1962.

12a. Neville, A.M. Properties of Concrete, chap. 1. Harlow: Longman Group; 1995.

13. Cotrell, S.P.; Halse, M.R.; Strange, J.H. NMR imaging of solids using large oscillating field gradients. Meas. Sci. Technol. 1:624–629; 1990.
14. Samoilenko, A.A.; Artemov, D.Y.; Sibeldina, L.A. Formation of a sensitive layer in experiments on NMR sub surface imaging of solids. JETP Lett. 47:417–419; 1988.
15. McDonald, P.J.; Perry, K.P.; Roberts, S.P. A repetitive pulse variant of broad line gradient echo magnetic resonance imaging. Meas. Sci. Technol. 4:896–898; 1993.
16. D'Orazio, F.; Bhattacharja, S.; Halperin, W.P.; Eguchi, K.; Mizusaki, T. Molecular diffusion and nuclear magnetic resonance relaxation of water in unsaturated porous silica glass. Phys. Rev. B 42:9810–9818; 1990.
17. Hall, C. Water sorptivity of mortars and concretes: a review. Magazine Concrete Res. 41:51–61; 1989.
18. Crank, J. The Mathematics of Diffusion, chapt. 7. Oxford, UK: Oxford University Press; 1975.